

available at www.sciencedirect.comjournal homepage: www.elsevier.com/locate/ejps

An improved *in vitro* model of human intestinal follicle-associated epithelium to study nanoparticle transport by M cells

Anne des Rieux^{a,b,1}, Virginie Fievez^{a,b,1}, Ivan Théate^c, Jan Mast^d,
Véronique Prémat^a, Yves-Jacques Schneider^{b,*}

^a Université catholique de Louvain, Unité de Pharmacie Galénique, Avenue E. Mounier, 73-20, 1200 Brussels, Belgium

^b Laboratoire de Biochimie cellulaire, Institut des Sciences de la Vie, Université catholique de Louvain, Croix du Sud, 5, 1348 Louvain-La-Neuve, Belgium

^c Department of Pathology, Cliniques Universitaires Saint-Luc, Université catholique de Louvain, Avenue Hippocrate 10, 1200 Brussels, Belgium

^d Centrum voor Onderzoek in Diergeneeskunde en Agrochemie, Groeselenberg, 99, 1180 Brussels, Belgium

ARTICLE INFO

Article history:

Received 20 October 2006

Received in revised form

13 December 2006

Accepted 29 December 2006

Published on line 13 January 2007

Keywords:

M cells

Follicle associated epithelium

Nanoparticles

Oral delivery of peptides

Caco-2

ABSTRACT

An alternative *in vitro* model of human follicle-associated epithelium (FAE) to study nanoparticle transport mechanisms by M cells was developed and characterized. The previous *in vitro* model of human FAE has been improved by inverting inserts after Caco-2 cell seeding. Raji and M cells were identified only in inverted co-culture cell monolayers by immunohistochemistry, confocal microscopy, and electron microscopy. The M cell conversion rate evaluated by scanning electron microscopy ranged between 15 and 30% of cells. Transport of 200 nm carboxylated polystyrene nanoparticles was higher and more reproducible in the inverted model. Nanoparticle transport was temperature-dependent, not affected by the presence of EGTA or by potassium depletion, but inhibited by EIPA or nystatin, suggesting that it occurs most likely by macropinocytosis. The inverted model appears more physiological, functional and reproducible than the normally oriented model.

© 2007 Elsevier B.V. All rights reserved.

1. Introduction

The intestinal epithelium consists of a cell monolayer, which is predominantly composed of enterocytes mixed, e.g., with mucus-secreting goblet cells; this layer constitutes an effective barrier that should prevent the entrance of microorganisms

and other particles into the organism. Organized mucosa-associated lymphoid tissue (O-MALT) is scattered throughout the gastrointestinal mucosa (Owen, 1977); this tissue consists of lymphoid follicles arranged either individually or in clusters to form distinct structures, such as Peyer's patches, situated immediately beneath the epithelial cell layer. In the intestine,

* Corresponding author. Tel.: +32 10 47 27 91; fax: +32 10 47 48 95.

E-mail address: yjs@uclouvain.be (Y.-J. Schneider).

Abbreviations: FAE, follicle associated epithelium; TEER, transepithelial electrical resistance; O-MALT, organized mucosa-associated lymphoid tissues; DMEM, Dulbecco modified Eagle's minimal essential medium; PEST, penicillin–streptomycin; PBS, phosphate-buffered saline; HBSS, Hank's balanced salt solution buffer; SEM, scanning electron microscopy; TEM, transmission electron microscopy; LDH, lactate dehydrogenase

¹ These authors have equally contributed to the work.

0928-0987/\$ – see front matter © 2007 Elsevier B.V. All rights reserved.

doi:10.1016/j.ejps.2006.12.006

these lymphoid structures are separated from the lumen by the follicle-associated epithelium (FAE), which differs from normal epithelium in that it contains, in addition to enterocytes and few goblet cells, specialized epithelial M cells with the capacity to transport particulate matter, such as bacteria and viruses. M cells are specialized for antigen sampling, but they are also exploited by many pathogens as a route of host invasion (Gebert and Bartels, 1995; Gebert et al., 1996). Due to their high transcytotic capacities and their ability to transport a broad range of materials, including nanoparticles (Frey et al., 1996; Neutra et al., 2003), these cells have become a promising research field, offering a putative way for oral delivery of nanoencapsulated therapeutic peptides and vaccines.

It has been shown that soluble tracers are endocytosed by M cells via fluid-phase endocytosis (Gebert and Bartels, 1995). Other soluble antigens, such as lectins, bind to receptors on the apical membrane of M cells and are taken up by receptor-mediated endocytosis (Gebert et al., 1996). In addition, M cells conduct clathrin-mediated endocytosis of ligand-coated particles (Frey et al., 1996), fluid-phase pinocytosis (Owen, 1977), actin-dependent phagocytosis (Beier and Gebert, 1998; Neutra et al., 2003), and macropinocytosis engulfment involving disruption of the apical cytoskeletal organization (Jones et al., 1994).

However, although the potentially useful properties of M cells on particle uptake are now well known and described, the mechanisms whereby particles are taken up and transported by M cells remain poorly understood. Due to the small number of M cells in the human gastrointestinal tract (5% of the human FAE, i.e., less than 1% of the total intestinal surface (Giannasca et al., 1999)), *in vivo* studies are difficult to perform and not always relevant due to the highly variable proportion and phenotype of M cells among different species (Jepson et al., 1996; Brayden and Baird, 2001). In addition, intestinal loops from anesthetized rodents have some inherent drawbacks (Brayden, 2001) and difficulty in maintaining differentiated primary intestinal M cells in culture, as well as the lack of *in vitro* models, has delayed progress in the understanding of M cell physiology and function (Niedergang and Kraehenbuhl, 2000).

Recently, *in vitro* models of human FAE have been developed. First, Kerneis et al. (1997) proposed a “mixed” co-culture system of Caco-2 cells and isolated lymphocytes from mouse Peyer’s patches on inverted culture inserts. Then, to avoid using primary murine lymphocytes, Gullberg et al. (2000) suggested a model based on co-culture of Caco-2 cells and human Raji B lymphocytes on normally oriented inserts. We previously used this FAE model to study the influence of M cells on the oral delivery of nanoencapsulated drugs (des Rieux et al., 2005). Our results, however, indicated that a more physiological model would be more useful. To achieve this goal, the inserts were inverted to make the Caco-2 cell monolayer more accessible to B lymphocytes and to encourage closer contacts between the two cell types (Honbo et al., 2004). This inverted model was characterized and compared with the model developed by Gullberg et al. (2000), in terms of functionality and reproducibility. Moreover, for the first time, as far as we know, the percentage of M cells present in the inverted *in vitro* model of the human FAE was evaluated. Finally, we studied the mechanisms of transport of model nanoparticles

(200 nm carboxylated polystyrene particles) by the inverted FAE model.

2. Materials and methods

2.1. Materials

2.1.1. Cell lines

Human colon carcinoma Caco-2 line (clone 1), obtained from Dr. Maria Rescigno, University of Milano-Bicocca, Milano, Italy (Rescigno et al., 2001), from passage $x + 12$ to $x + 30$, and human Burkitt’s lymphoma Raji B line (American Type Culture Collection, Manassas, VA) from passages 102–110 were used.

2.1.2. Cell culture media, chemicals, nanoparticles and antibodies

Dulbecco modified Eagle’s minimal essential medium (DMEM, 25 mM glucose), RPMI 1640 medium, nonessential amino acids, L-glutamine and penicillin–streptomycin (PEST) were purchased from Gibco™ Invitrogen Corporation (Carlsbad, CA). Heat inactivated fetal calf serum was obtained from Hyclone (Perbio Sciences, Erembodegem, BE). Trypsin-EDTA consisted of 2.5% (w/v) trypsin (Gibco™) and 0.2% (w/v) EDTA (IGN, Aurora, OH) in phosphate-buffered saline (PBS, Gibco™). Hank’s balanced salt solution buffer (HBSS), PBS with or without calcium and magnesium were obtained from Gibco™. Rhodamine-phalloidin was obtained from Molecular Probes (Eugene, OR). Nystatin was purchased from Sigma (St. Louis, MO), as well as 5-(N-ethyl-N-isopropyl) amiloride (EIPA), ethylene glycol-bis(β -aminoethyl ether)-N,N,N’,N’-tetraacetic acid tetrasodium salt (EGTA). For the potassium depletion study, HBSS without potassium was prepared with 140 mM NaCl, 1 mM CaCl₂, 1 mM MgCl₂, 20 mM HEPES and 5.5 mM glucose, pH 7.4. Glutaraldehyde was purchased from Merck (Darmstadt, GE). Transwell® polycarbonate inserts (12 wells, pore diameter of 3 μ m, polycarbonate) were purchased from Corning Costar (New York, NY). Inserts were coated with Matrigel™ Basement Membrane Matrix (Becton Dickinson, Bedford, MA). Yellow-green carboxylated latex particles (FluoSpheres®) with a mean diameter of 200 nm were obtained from Molecular Probes. The silicon tubes (internal \varnothing 14 mm) came from Labo-Moderne (Paris, FR). Petri dishes (glass, $\varnothing \times h$ (mm) = 200 \times 50) were purchased from VWR (Leuven, BE). ¹⁴C-Mannitol was from GE Healthcare (Chalfont St. Giles, UK). The CellTrace™ Carboxyfluorescein succinimidyl ester (CFSE) Cell Proliferation kit was obtained from Molecular Probes. The anti-B cell specific activator protein (BSAP) antibody was purchased from BD transduction Lab. The Envision system was from Dako (Glostrup, DK). Fluorescein-isothiocyanate (FITC)-dextran, 4 kDa and 12 kDa, and diaminobenzidine (DAB), were purchased from Sigma. The LDH activity was measured with a kit from Roche (Vilvoorde, BE) (ref. 1 644 793).

2.2. *In vitro* model of the human FAE

Caco-2 cells were grown in flasks in DMEM supplemented with 10% (v/v) fetal calf serum, 1% (v/v) non-essential amino-acids, and 1% (v/v) L-glutamine, at 37 °C under a 10% CO₂ water saturated atmosphere. Caco-2 cells were grown on inserts in the

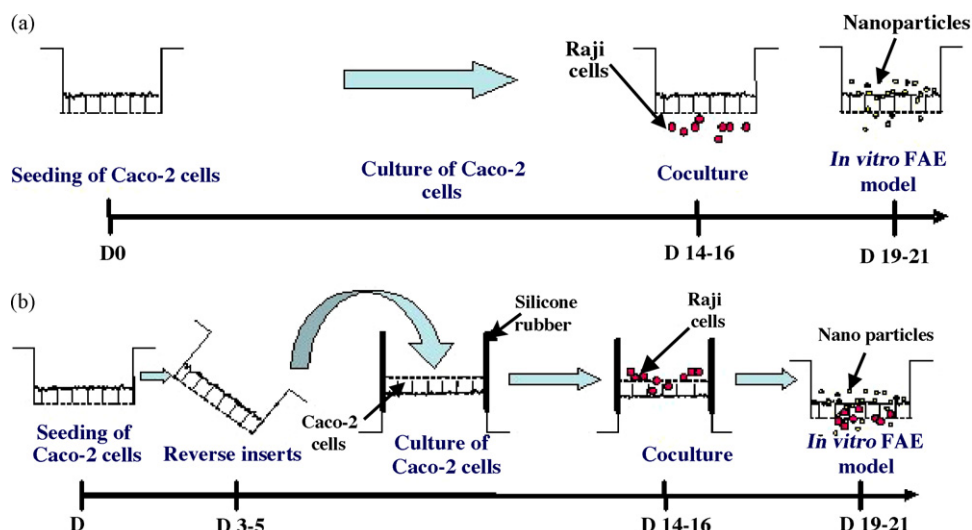


Fig. 1 – Time scale of the protocol developed to obtain an optimized inverted in vitro FAE model.

same medium, further supplemented with 1% (v/v) PEST. Raji cells are non-adherent cells and perform as a suspension culture both in the normally and inverted co-culture models. They were cultivated in RPMI supplemented with 10% (v/v) fetal calf serum, 1% (v/v) non-essential amino-acids, 1% (v/v) L-glutamine, and 1% (v/v) PEST, at 37 °C in a 5% CO₂ water saturated atmosphere.

The normally oriented FAE model was obtained following the protocol developed by Gullberg et al. (Gullberg et al., 2000; des Rieux et al., 2005) (Fig. 1a). Briefly, Transwell® inserts were coated with Matrigel™, prepared in pure DMEM to a final protein concentration of 100 µg/ml; 300 µl of this solution was poured onto the inserts (30 µg/cm²), which were then placed at room temperature for 1 h. Supernatants were then removed and inserts washed with 500 µl of DMEM. Five hundred thousand Caco-2 cells, suspended in 500 µl of supplemented DMEM + 1% (v/v) PEST, were seeded on the upper insert side and cultivated for 14 days. Five hundred thousand Raji cells, in supplemented DMEM + 1% (v/v) PEST, were then added to the basolateral insert compartment. The co-cultures were maintained for 4–5 days (Fig. 1a). The upper compartment medium was changed every other day. Mono-cultures of Caco-2 cells, cultivated as above but without the Raji cells, were used as controls.

The inverted FAE model was obtained by adapting an existing protocol (Honbo et al., 2004) (Fig. 1b). Cells were cultivated as described above but, 3–5 days after Caco-2 cell seeding, the inserts were inverted in Petri dishes filled with supplemented DMEM + 1% (v/v) PEST; a piece of silicon tube was then placed on the basolateral side of each insert and was filled with supplemented DMEM + 1% (v/v) PEST. Inverted inserts were cultivated for 9–11 days and the basolateral compartment medium was changed every other day. Raji cells, resuspended in supplemented DMEM + 1% (v/v) PEST, were then added to the basolateral compartment of the inserts. The co-cultures were maintained for 5 days. Mono-cultures of Caco-2 cells, cultivated as above but without the Raji cells, were used as controls. Before the experiments, the silicon tubes were

removed, and the cell monolayers placed in multiwell plates and washed twice in HBSS. Inserts were used in their original orientation for all the following experiments.

2.3. Validation and characterization of the inverted in vitro model of human FAE

2.3.1. Assessment of cell monolayer integrity

Cell monolayer integrity, both in co- and mono-cultures, was controlled by measurement of transepithelial electrical resistance (TEER) and by evaluation of cell permeability to ¹⁴C-Mannitol and FITC-dextran (4 and 12 kDa).

Cell monolayers were washed twice in HBSS, unless stated otherwise, and allowed to equilibrate for 30 min at 37 °C before TEER measurements. Cell monolayer TEER was measured in HBSS at 37 °C with an Endohm™ tissue resistance chamber (Endohm-12, World Precision Instruments, Sarasota, FL) connected to a Millicell®-RES (Millipore, Billerica, MA.) ohmmeter. The resistance of HBSS alone (9 Ωcm²) was considered as background resistance and subtracted from each TEER value. TEER values were measured before and after the transport experiments.

The integrity of the cell monolayer tight junctions was controlled by evaluation of the permeability to ¹⁴C-mannitol and 4 or 12 kDa FITC-dextran in transport conditions (HBSS) and in the presence of EGTA. Donor solutions were prepared by diluting ¹⁴C-mannitol and FITC-dextran in HBSS to a final concentration of 0.9 µCi/ml or 0.1 mM, respectively, and were added apically to cell monolayers (400 µl). In transport conditions (HBSS), inserts were incubated at 37 °C for the required duration and basolateral solutions were then sampled. To open the cellular tight junctions, inserts were incubated apically and basolaterally with 2.5 mM EGTA in HBSS, pH 7.4, for two 15 min periods at 37 °C before TEER measurements. A fresh EGTA solution was then placed basolaterally and FITC-dextran (4 or 12 kDa,) or ¹⁴C-mannitol were added apically (400 µl). Inserts were incubated for 1 h at 37 °C. Basolateral solutions were then sampled and analyzed.

The amount of transported ^{14}C -mannitol was measured by liquid scintillation; that of 4 or 12 kDa FITC-dextran by fluorimetry (485/530 nm) and the results were expressed as apparent permeabilities. Before to calculate apparent permeability coefficients (P_{app} , cm s^{-1}), the steady state condition of mannitol and dextran transport was checked. P_{app} were calculated using the following equation:

$$P_{\text{app}} = \frac{\Delta Q}{\Delta t} \times \frac{1}{A \times C_0}$$

where $\Delta Q/\Delta t$ is the amount of ^{14}C -mannitol or FITC-dextran transported in the basolateral compartment per time unit (t). Transport rates were calculated by plotting the amount of ^{14}C -mannitol or FITC-dextran transported to the basolateral side versus time and then by determining the slope of the plot. C_0 is the initial concentration in the donor compartment. A is the surface area of the Caco-2 monolayer ($A = 1.13 \text{ cm}^2$). Results are expressed as mean \pm standard error of the mean (S.E.M.).

2.3.2. Localization of Raji cells in co-culture monolayers

Two methods were used to identify and localize Raji cells within the cell monolayers. First, Raji cells were labeled yellow–green fluorescent with a CellTrace™ CFSE Cell Proliferation Kit (excitation 492 nm and emission 517 nm) according to the supplier's instructions, 3 days before incubation with Caco-2 cells (co-cultures). Briefly, a 5 mM CellTrace™ CFSE stock solution was prepared immediately prior to use by dissolving the content of one vial in 18 μl of dimethyl sulfoxide (DMSO). 10×10^6 Raji cells were centrifuged and the supernatant was removed. The 5 mM CFSE stock solution was diluted in PBS to 10 μM . Cells were gently suspended in pre-warmed (37 °C) PBS containing the probe, incubated for 15 min at 37 °C, re-centrifuged and suspended in fresh pre-warmed medium. Finally, Raji cells were incubated for another 30 min to ensure complete probe modification and washed again. Three days later, co-cultures were prepared as described: 14 days after Caco-2 cell seeding, fluorescent Raji cells were added to the basolateral pole of the inserts and the co-cultures were maintained for 5 days. Inserts were then washed three times in PBS, fixed in 4% (v/v) formaldehyde and washed again in PBS. Actin was stained with 250 μl of rhodamine-phalloidin (4 U/ml) in HBSS + 0.2% (v/v) Triton X-100 for 10 min to reveal cell borders. After washing in HBSS, the inserts were cut and mounted on glass slides. Mono- and co-cultures were observed with a DMIRE2 Leica confocal microscope (Wetzlar, GE) to localize Raji cells within the cell monolayers. Data were analyzed by Leica confocal software to obtain y - z and x - y views of cell monolayers. To confirm the correlation between yellow–green fluorescence and Raji cells, 5 μM of TOTO-3, for nucleus labeling, was added to the mounting medium. Mono-cultures were used as controls.

Second, Raji cells were identified and localized by immunohistochemistry. Inserts were fixed in 4% formalin, and then cut with a razor blade into thin sheets that were placed in Agar gel and embedded in paraffin. Five micrometers thick sections were cut and, after paraffin removal by xylene, were rehydrated and boiled for 75 min in 0.01 M citrate buffer 0.05% (v/v) Triton X-100, pH 5.8 with a water bath. Endogenous peroxidase activity was blocked by incubating in 0.3% H_2O_2 for 30 min and non-specific antibody staining was pre-

vented by preincubation in 10% (v/v) normal goat serum for 30 min. Sections were then incubated with anti-B cell specific activator protein (BSAP) monoclonal antibody (1:100) at 4 °C overnight and revealed using the Envision system with diaminobenzidine (DAB). Finally, samples were counterstained with hematoxylin, mounted, and examined with an AxioVision 3.1 microscope (Zeiss, Göttingen, GE) equipped with an AxioCam HRc digital camera (Zeiss). In addition, sections of normally oriented and inverted cell monolayers were stained with Hematoxylin-Eosin.

2.3.3. Quantification of Raji cells in co-cultured cell monolayers

The proportion of Raji cells located in the cell monolayer was evaluated by flow cytometry. Raji cells were labeled with CFSE and co-cultured as described above. Cell monolayers were washed twice in HBSS and incubated apically and basolaterally with a 5% (w/v) Trypsin-EDTA solution at 37 °C. Cells were then gently detached and filtered on 80 μm nylon filters. Cell suspensions were analyzed by flow cytometry (FACScan, Becton Dickinson) with 488 nm excitation and emission filters appropriate for fluorescein; differentiation of Caco-2 and Raji cells was based on fluorescence and size. The number of Raji cells was expressed as a percentage of the total number of counted Caco-2 and Raji cells. Mono-cultures were used as controls.

2.3.4. Presence and quantification of M cell co-cultures

Cells morphologically similar to M cells were discriminated from Caco-2 cells using transmission electron microscopy (TEM) and scanning electron microscopy (SEM). TEM and SEM were used to evaluate morphological changes of cells after co-culture with Raji cells. Mono- and co-cultures were washed twice in HBSS and fixed in 4% (v/v) formaldehyde/2% (v/v) glutaraldehyde. Ultra-thin sections of cell-covered filters were prepared for TEM analysis by standard methods, as described (Mast et al., 2005). Observations were made using a Philips EM208S TEM (FEI, Eindhoven, NE). Samples processed for SEM analysis were dehydrated, dried at critical point and gold-coated. Pictures of cell monolayers were obtained with a DMS 982 Gemini SEM (Zeiss).

Since no human-specific marker of M cell has yet been identified, discrimination of M cells within cell monolayers was based on morphological criteria. The microvilli-free morphology of M cells was used to identify and quantify them by SEM. The proportion of M cells was evaluated by measuring the surface (μm^2) represented by cells morphologically similar to M cells (no or fewer and shorter microvilli) as a function of the total surface analyzed (9869 μm^2). Five co-cultures were examined in four different random localizations selected by two persons. The cell surface was evaluated using AxioPlan software (Zeiss). Mono-cultures were used as controls.

2.4. Nanoparticle transport

2.4.1. Assessment of model functionality by nanoparticle transport experiments

Transport experiments were run in HBSS. Nanoparticle transport was studied at 37 °C, unless stated otherwise. Nanoparticle concentration was adjusted by diluting the stock

solution (checked by FACS analysis) in HBSS to a final concentration of 4.5×10^9 nanoparticles/ml and then vortexed for 1 min to dissociate possible aggregates. After equilibration in HBSS at 37 °C (unless stated otherwise), the apical medium of the cell monolayers was replaced by a nanoparticle suspension (400 μ l) and inserts were incubated at 37 °C (unless stated otherwise) for the required duration. Basolateral solutions were then sampled and the number of transported nanoparticles measured using a flow cytometer (FACScan, Becton Dickinson) (Gullberg et al., 2000; des Rieux et al., 2005). Results were expressed as percentages of the donor solution. Nanoparticle transport was expressed as mean \pm S.E.M.

2.4.2. Transcytosis mechanisms of nanoparticle transport by M cells

2.4.2.1. *Transcellular transport.* Inserts were incubated apically and basolaterally with 2.5 mM EGTA (in HBSS, pH 7.4) twice for 15 min at 37 °C. Tight junction opening was checked by TEER measurement. Fresh EGTA was then placed basolaterally and the nanoparticle suspension (4.5×10^9 nanoparticles/ml in HBSS) was added to the apical side of the cell monolayers (400 μ l). Inserts were incubated for 1 h at 37 °C and basolateral solutions were then sampled and analyzed. The number of transported nanoparticles was measured using a flow cytometer (Gullberg et al., 2000; des Rieux et al., 2005). The absence of cytotoxicity in the presence of EGTA was assessed by measuring the lactate dehydrogenase (LDH) activity released from the cytosol of damaged cells into the apical medium.

2.4.2.2. *Energy dependent mechanism.* The transport of 200 nm carboxylated polystyrene nanoparticles by mono- and co-cultures was evaluated at 4, 10, 16 and 37 °C. Inserts were pre-incubated for 15 min in HBSS at different temperatures. The nanoparticle suspension, first preincubated at the desired temperature, was added to the apical side of the cell monolayers (400 μ l) and inserts were incubated at 4, 10, 16 or 37 °C for 30 min. Finally, basolateral solutions were sampled and the number of transported particles was measured using a flow cytometer (Gullberg et al., 2000; des Rieux et al., 2005). Results were expressed as percentages of the donor solution.

2.4.2.3. *Endocytosis mechanism.* In order to determine by which mechanism carboxylated nanoparticles were transported, transport experiments were conducted with inhibitors of macropinocytosis (nystatin and EIPA) and in potassium depleted conditions that inhibit clathrin-mediated endocytosis.

For inhibition experiments, cell monolayers were first preincubated apically with 150 μ l of inhibitor in HBSS (nystatin 11 μ M, EIPA 50 μ M (Ragnarsson, 2006)) for 20 min at 37 °C, before adding the nanoparticle suspension. The inhibitor was present throughout the nanoparticle transport experiment. The absence of cytotoxicity in the presence of inhibitors was assessed by measuring the LDH activity released from the cytosol of damaged cells into the apical medium after the transport experiments.

Potassium depletion was performed according to Madshus et al. (1987a, 1987b). After TEER measurement, cell monolayers were submitted to a 5 min hypotonic shock in DMEM/H₂O

(1:1) at 37 °C. Cells were rinsed once with HBSS devoid of potassium and incubated in this medium for 1 h at 37 °C. TEERs were measured and apical and basolateral media were removed. Nanoparticles suspended in HBSS devoid of potassium were added apically (400 μ l) while HBSS devoid of potassium was added basolaterally. Cell monolayers were incubated for 1 h at 37 °C. Basolateral solutions were then sampled and the number of transported particles was measured using a flow cytometer (Gullberg et al., 2000; des Rieux et al., 2005).

2.5. Statistics

Differences among treated groups were analyzed using a Mann–Whitney non-parametric test (significance $P < 0.05$).

3. Results and discussion

3.1. Validation and characterization of the inverted in vitro model of human FAE

Before performing transepithelial transport experiments, the inverted *in vitro* model first needed to be validated and characterized. The integrity and functionality of the cell monolayer, as well as the presence of M cells, were compared in both the normal and the inverted model.

3.1.1. Cell monolayer integrity

3.1.1.1. *Inverted model.* A drawback of *in vitro* FAE models is the decrease in TEER observed after 5 days of co-culture, and hence the possible deterioration in tight junction function. TEER decrease is considered to be a result of Caco-2 cell conversion into M cells (Gullberg, 2005). Reduction of the inverted co-culture TEER was a first sign of this conversion, and raised the question of tight junction integrity. To test the barrier function of the tight junctions, the P_{app} s of paracellular markers (mannitol and 4 and 12 kDa dextrans) (Riley et al., 1991; Sakai et al., 1997) were evaluated in HBSS and in the presence of 2.5 mM EGTA, a calcium chelator (Mounier et al., 1992; Knipp et al., 1997; Sergent et al., 2006) that opens tight junctions (Fig. 2A). The P_{app} s of mannitol and dextrans were higher for co- than for mono-cultures. Co-culture tight junctions may be less tight than those of mono-cultures but, considering the increased ability of co-cultures to perform endocytosis, these molecules may also cross the epithelial barrier by transcytosis. However, addition of EGTA induced a systematic increase in the P_{app} , demonstrating that the tight junctions were functioning and able to open under EGTA action. Finally, the higher the molecular weight, the lower the P_{app} . These data indicate that mono- and co-culture intercellular junctions remained tight.

3.1.1.2. *Comparison of normal and inverted model.* In both the normally oriented and inverted models, mannitol P_{app} s were four-fold higher in co- than in mono-cultures, and they were two-fold higher in inverted co-cultures than in normally oriented co-cultures (Fig. 2B). However, the P_{app} values remained in the range (10^{-6} cm s⁻¹) reported in the literature for Caco-2 cell monolayers with good tightness (Artursson et al., 2001). The mannitol P_{app} s of normally oriented and

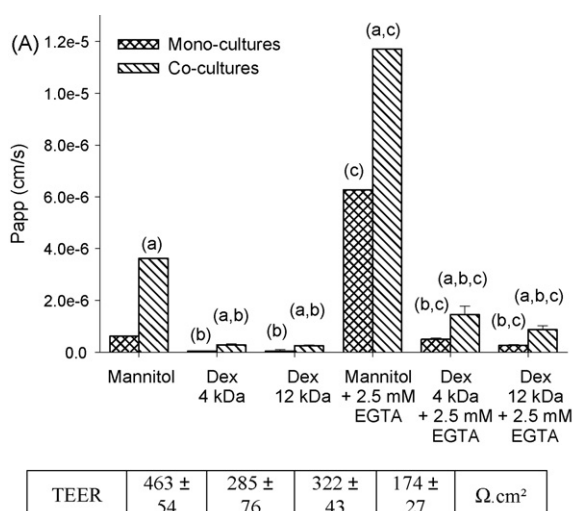


Fig. 2 – In vitro model characterization. (A) Cell monolayer integrity of the inverted model. ^{14}C -mannitol, 4 and 12 kDa FITC-dextrans have been incubated with inverted mono- and co-culture for 60 min at 37 °C ($n = 3$), either in HBSS or with 2.5 mM EGTA in HBSS. Dex stands for Dextran. ^{14}C -mannitol was quantified by liquid scintillation and dextrans by fluorimetry. (a) $P < 0.05$ vs. corresponding P_{app} of mono-cultures (b) $P < 0.05$ vs. corresponding P_{app} of mannitol; (c) $P < 0.05$ vs. corresponding P_{app} without EGTA. (B) Comparison of the normally oriented and inverted FAE models. 4.5×10^9 nanoparticles/ml (0.2 μm FITC-labelled carboxylated nanoparticles) and 0.9 $\mu\text{Ci/ml}$ of ^{14}C -mannitol, suspended in HBSS, were added to the apical pole of the cell monolayers. Mono- and co-cultures were incubated with the cell monolayers for 60 min at 37 °C ($n = 5$). The number of transported nanoparticles was evaluated by flow cytometry and the amount of transported ^{14}C -mannitol was measured by liquid scintillation. TEER values appear above each group results. (a) $P < 0.05$ (nanoparticles and mannitol P_{app}) vs. mono-cultures; (b) $P < 0.05$ (nanoparticles and mannitol P_{app}) vs. normally oriented co-cultures.

inverted mono-cultures were not significantly different. Thus, mono- and co-cultures retained a significant barrier function.

The TEER difference between mono- and co-cultures that has already been described (Gullberg et al., 2000; des Rieux

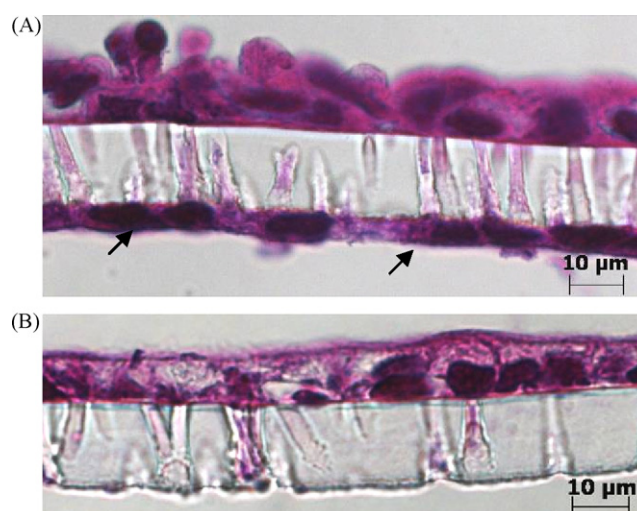


Fig. 3 – Comparison of the normally oriented and inverted cell monolayers sections of normally oriented (A) and inverted (B) cell monolayers were stained with hematoxylin-eosin. The presence of cells growing on the basolateral side of the insert was put in evidence (black arrows).

et al., 2005) was observed both in normal and in inverted inserts (Fig. 2B). The TEERs of normally oriented inserts were slightly higher than those of inverted inserts. The increased TEER of normally oriented inserts may have resulted from the presence of Caco-2 cells on the lower insert side as evidenced by histology (Fig. 3). When seeded on inserts with 3 μm pores, Caco-2 cells can cross the membrane and grow on the basolateral side of the insert membranes. Inverting the inserts decreased this phenomenon, which may also explain the slightly higher mannitol permeability of inverted inserts.

3.1.2. Localization and quantification of Raji cells in co-cultured cell monolayers

Aiming for a more physiological model, we expected that inverting inserts would induce Raji penetration within the cell monolayers and thus allow direct contact between Caco-2 and Raji cells. The presence or absence of direct contact between Raji and Caco-2 cells was explored in the two models. Raji cells were localized by confocal microscopy and by immunohistochemistry. Quantification of the Raji cells found within the cell monolayers was performed by flow cytometry. Mono- and co-cultures of normally oriented and inverted inserts were compared.

Fluorescent labeling and confocal analysis allowed cell borders (red) and nuclei (blue) to be visualized (Fig. 4a). When analyzing inverted co-cultures, Raji cells (yellow-green) were observed within the enterocyte layer (Fig. 4b), xz views showing Raji cell localization within the co-culture cell monolayers. Double staining of the nucleus and cytoplasm of Raji cells demonstrated that the yellow-green fluorescence belonged to Raji cells and was not the result of free fluorescence accumulation (Fig. 4c). No Raji cells were detected in mono-cultures (Fig. 4d). In addition, in agreement with Gullberg et al. (2000), confocal analysis of normally oriented co-cultures clearly

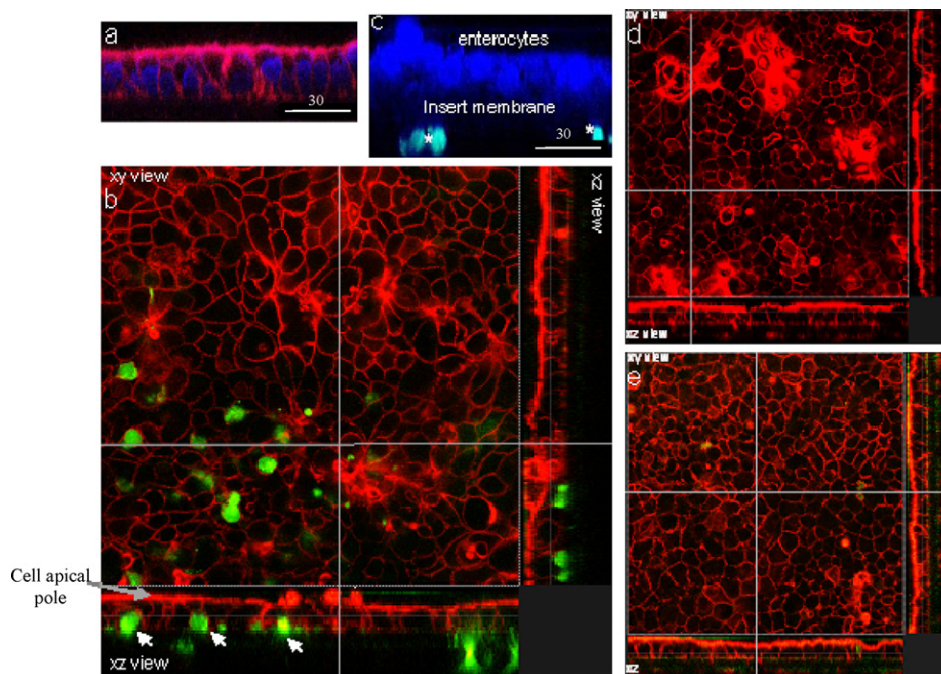


Fig. 4 – Display of Raji cells within co-cultures by confocal analysis. Enterocyte actin was stained with rhodamine-phalloidin (red) and Raji cells were CFSE-labelled (yellow–green). Inverted (b)–(d) and normally oriented co-cultures (e) were fixed after 5 days of incubation with CFSE-labelled Raji cells. Mono-cultures were used as control (a) and (d). White arrows indicate the Raji localization in the cell monolayers. To confirm the correlation between the yellow–green fluorescence and the presence of Raji cells in the co-cultures, 5 μ M of TOTO-3 (blue color), labelling the cell nuclei, were added in the mounting medium (c). Turquoise blue color resulted from the merge of blue and yellow–green fluorescence (white star). Mono-cultures were used as controls (a). Grey lines indicate where, within the cell monolayers, the pictures were taken and analyzed. (For interpretation of the references to colour in this figure legend, the reader is referred to the web version of the article.)

showed that no Raji cells were present in the cell monolayers (Fig. 4e).

The presence of Raji cells in inverted co-cultures was corroborated by immunohistochemistry. Examination of paraffin sections revealed the presence and localization of Raji cells (brown) below inserts, but also within the cell monolayers (blue) (Fig. 5).

The percentage of Raji cells in inverted co-cultures was evaluated to range between 17 and 30% of the total number of detected cells (Caco-2 and Raji cells) (mean = $22.45 \pm 1.6\%$, $n = 8$). FACS analysis confirmed the confocal microscopy observations, since no Raji cell was detected in mono-cultures (both normally oriented and inverted) or in normally oriented co-cultures ($n = 5$).

In conclusion, close contact between Raji and Caco-2 cells was only observed for inverted co-cultures, which, therefore, reflect the human FAE more closely than the normally oriented co-cultures.

3.1.3. Assessment of M cell presence and evaluation of the percentage of M cells in inverted co-cultures

To complete the inverted human FAE model characterization, it seemed essential to provide evidence of the presence of converted M cells within the cell monolayers. In the absence of any specific marker of human M cells, the discrimination between Caco-2 and M cells was done on a morphological basis. M cells show a reduced brush border as well as an invaginated baso-

lateral membrane, forming a pocket to welcome immune cells (Gebert et al., 1996). The particular shape of their apical membrane was used to identify cells morphologically similar to M cells by TEM and SEM.

Mono- and co-cultures were analyzed by TEM. While enterocyte-like cells with a well developed brush border were observed in mono-cultures (Fig. 6A, a), cells without microvilli were visualized in co-cultures (Fig. 6A, b), although desmosomes between them and adjacent cells suggest their enterocytic origin (Fig. 6A, c). Moreover, underlying these enterocytes, cells were observed that could have been Raji cells based on their relatively condensed chromatin and their lack of desmosomes (Fig. 6A, b). These observations indicated that at least some of the Caco-2 cells had converted into M cells.

These results were confirmed by SEM analysis of mono- and co-cultures. SEM has already been used to identify and localize M cells in Peyer's patch biopsies (Gebert, 1997) and in the *in vitro* FAE model (Schulte et al., 2000) developed by Kerneis et al. (1997). Analyzing cell monolayers in the inverted FAE model, SEM revealed that some Caco-2 cells, after 5 days co-culture, expressed short and irregular microvilli (Fig. 6B, c and d), whereas, in mono-cultures, all differentiated Caco-2 cells displayed a regular brush border and well-developed tight junctions (Fig. 6B, a and b). In co-cultures, two types of cells can be distinguished on the basis of surface structures: enterocyte-like cells with a regular brush border, and M-like cells with a less regular arrangement of microvilli than enterocyte-like

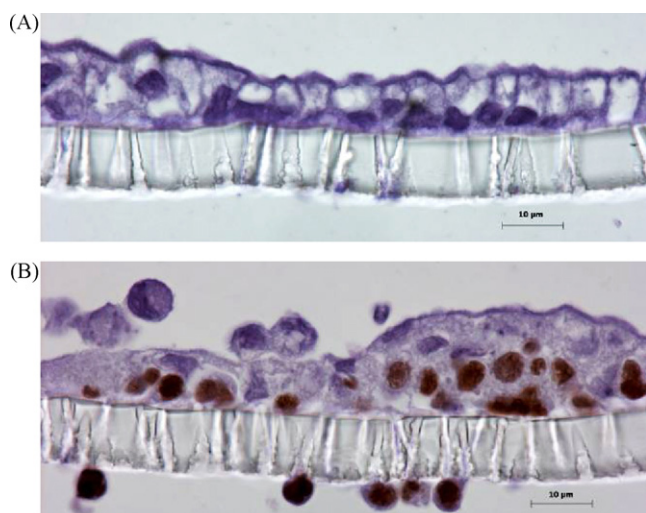


Fig. 5 – Localization of Raji cells in co-culture cell monolayers by immunohistochemistry. Sections of mono- and co-cultures were incubated with the BSAP monoclonal antibody and revealed with DAB (brown) (counterstained with haematoxylin (blue)). Mono-cultures were used as controls. (A) Inverted mono-cultures and (B) inverted co-cultures. (For interpretation of the references to colour in this figure legend, the reader is referred to the web version of the article.)

cells. No cell with few or sparse microvilli were observed in the mono-cultures.

As far as we know, the percentage of M cells present within co-cultures of Caco-2 and Raji cells has never been evaluated. This information is of outmost importance to interpret *in vitro* results and to put them in context with the *in vivo* situation. Cells with few or no microvilli were identified as cells morphologically comparable to M cells by SEM and their proportion was evaluated. The surface occupied by cells morphologically similar to M cells in the co-cultures was evaluated to range between 15 and 30% (mean = $22.87 \pm 2.4\%$, $n = 5$). As mentioned above, no cells with few or sparse microvilli were observed in the mono-cultures.

Hence, in the inverted *in vitro* model of human FAE, 15–30% of the Caco-2 cells were converted to M cells, assuming a surface equivalence for M and Caco-2 cells.

3.2. Transport of nanoparticles by M cells

3.2.1. Nanoparticle transport

3.2.1.1. Inverted model. The most remarkable and interesting property of M cells is their high transcytotic capacity and their ability to transport a broad range of materials, including nanoparticles (Frey and Neutra, 1997; Clark et al., 2000). To monitor the conversion of Caco-2 cells into M cells, the transport rate of 200 nm carboxylated polystyrene nanoparticles across inverted mono- and co-cultures was studied (Gullberg et al., 2000). The number of transported nanoparticles after 60 min of incubation at 37 °C was significantly higher in co-cultures than in mono-cultures ($38,900 \pm 5600$ versus 806 ± 510 nanoparticles, respectively;

$n = 5$, $P < 0.05$), establishing the conversion of Caco-2 cells into M cells.

3.2.1.2. Comparison of normal and inverted models. Both models were functional, although nanoparticle transport in normal co-cultures was only 3-fold higher than in mono-cultures whereas it was 50-fold higher in inverted co-cultures (Fig. 2B). Hence, inverted co-cultures were more efficient at transcytosing nanoparticles than normally oriented cultures. No significant difference was observed between the nanoparticle P_{appS} for normal and inverted mono-cultures ($n = 5$).

In addition, the inter-experiment coefficient of variation of normally oriented co-cultures was systematically (five independent experiments) larger than the coefficient of variation of inverted co-cultures (121 and 55% on average for normally oriented and inverted co-cultures, respectively). The intra-experiment coefficient of variation (five independent inserts) of normally oriented co-cultures was also higher than for inverted co-cultures (95 and 14% for normally oriented and inverted co-cultures, respectively).

In conclusion, by inverting the inserts, a more physiological, functional and reproducible *in vitro* model of human FAE has been obtained to study nanoparticle transport.

3.2.2. Transcytosis mechanisms of nanoparticle transport

In order to determine by which mechanism(s) the 200 nm carboxylated polystyrene nanoparticles were transported by M cells across cell monolayers, several experiments were performed.

To verify that nanoparticle transport by M cells was transcellular, inverted cell monolayers were incubated in the presence of 2.5 mM EGTA to induce the opening of enterocyte tight junctions. Nanoparticle transport was not increased in the presence of EGTA and was even lower in co-cultures (53 ± 13 versus 87 ± 41 nanoparticles/h for mono-cultures and $24,450 \pm 7130$ versus $15,880 \pm 2300$ nanoparticles/h for co-cultures, $n = 5$). These results suggest, therefore, that 200 nm carboxylated polystyrene nanoparticles were not transported by the paracellular route. Most probably these nanoparticles are too large to be transported by this route, even when the tight junctions are open. Moreover, nanoparticles are composed of polystyrene, a polymer unable to open cell tight junctions, unlike chitosan (Artursson et al., 1994).

Nanoparticle transport by M cells is known to be predominantly mediated by endocytosis, an energy-dependent mechanism (Gebert et al., 1996). To evaluate if this mechanism was also involved for M cells in the inverted model, transport rates at 4, 10, 16 and 37 °C were compared (Fig. 7). At 4 °C, nanoparticle uptake should be inhibited (Kerneys et al., 1997; Gullberg et al., 2000; des Rieux et al., 2005), whereas at 10 °C deep invagination of the pits occurs, but internalization is still prevented (Beaumelle et al., 1990), thus inhibiting nanoparticle endocytosis. Above 16 °C, nanoparticle endocytosis by M cells is no longer inhibited (Ellinger et al., 2002; Zaro and Shen, 2005). The number of transported nanoparticles in co-cultures was significantly higher than in mono-cultures, regardless of the temperature. Nanoparticle transport by mono-cultures was not influenced by temperature. For the co-cultures, transport rates at 16 and 37 °C were comparable, and were increased

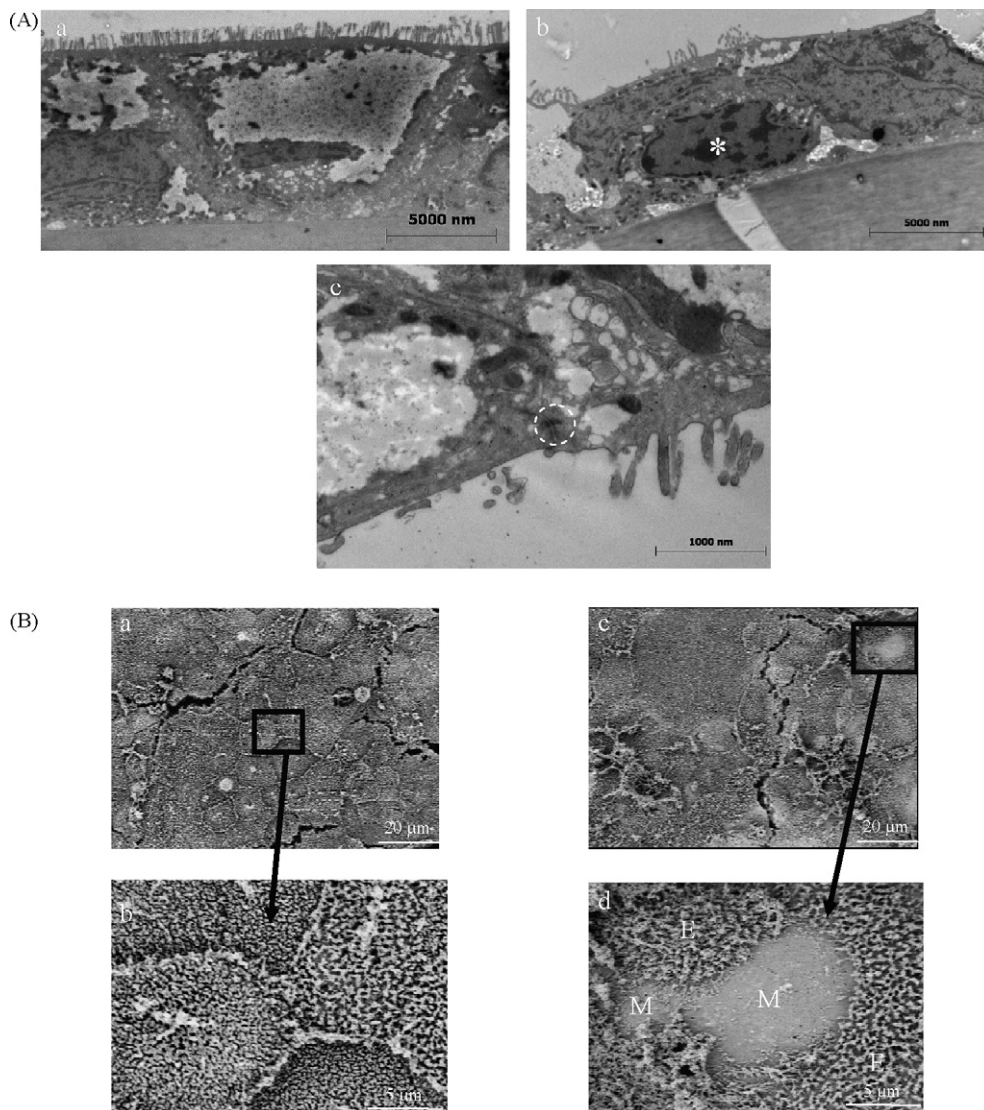


Fig. 6 – Identification of M cells by microscopy. (A) TEM analysis. Cell monolayers were fixed and processed for TEM analysis. Mono-cultures present a columnar shape as well as a brush border (a). M cells were identified by their lack of microvilli at their apical surface (b) and the presence of desmosomes (c, with circle). A cell that could be identified as a Raji lymphocyte based on its relatively condensed chromatin and its lack of desmosomes between its membrane and that of adjacent enterocytes, lies under the enterocyte monolayer (b, white star). (B) SEM analysis. Cell monolayers were fixed and processed for SEM analysis. M cells were identified by their lack or fewer microvilli at their apical surface (c) and (d). Mono-cultures were used as control (a) and (b).

about 10-fold compared to transport rates at 4 and 10°C (not significantly different).

Whether the internalization of nanoparticles by M cells occurs by macropinocytosis or receptor-mediated endocytosis remains largely unknown. In order to investigate the mechanisms of nanoparticle transcytosis by M cells, nanoparticle transport was studied in the inverted *in vitro* model of human FAE, in the presence of classical endocytosis inhibitors, i.e. EIPA and nystatin, and in the absence of potassium. EIPA has been used as a selective inhibitor of macropinocytosis (Wadia et al., 2004; Fallman and Gustavsson, 2005), although the exact mechanism of inhibition is not well understood. It has been suggested that EIPA inhibits the cell membrane

Na⁺/H⁺ exchange protein (Pizarro-Cerda and Cossart, 2004), altering intracellular pH and thus inducing alterations in the cytoskeleton (Peachman et al., 2004), or in other processes related to macropinocytosis (Liu et al., 1993). Nystatin disrupts lipid-raft mediated pathways, including caveolae and macropinocytosis, by removing cholesterol from membranes (Liu et al., 2002; Wadia et al., 2004). Since Larkin et al. (1983) have demonstrated that a depletion in intracellular potassium reversibly arrests coated pit formation and receptor-mediated endocytosis in human fibroblasts, experiments to determine whether nanoparticles were transported by a clathrin-associated pathway, were conducted in intracellular potassium depletion conditions.

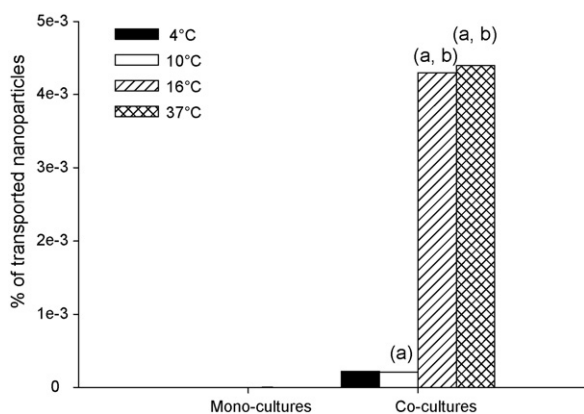


Fig. 7 – Is transport of nanoparticles by M cells energy-dependent? Mono- and co-cultures were incubated in HBSS at 4, 10, 16 and 37 °C and 4.5×10^9 nanoparticles/ml ($0.2 \mu\text{m}$ FITC-labelled carboxylated nanoparticles), suspended in HBSS, pre-incubated at 4, 10, 16 and 37 °C, were added to apical pole of cell monolayers. Mono- and co-cultures were incubated with cell monolayers for 60 min at 37 °C ($n = 4$ and 8 for monocultures and co-cultures, respectively). The number of transported nanoparticles was evaluated by flow cytometry. (a) $P < 0.05$ vs. mono-cultures (b) $P < 0.05$ vs. co-cultures when incubated at 4 and 10 °C.

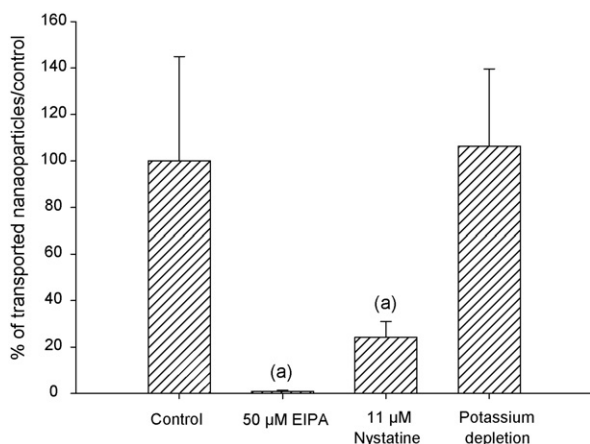


Fig. 8 – Mechanistic characterisation of nanoparticle transport by M cells. Endocytosis inhibitors: cell monolayers were first apically pre-incubated with inhibitors (EIPA and nystatin) in HBSS for 20 min at 37 °C, before adding nanoparticle suspension ($n = 4$). Inhibitor was present throughout the whole nanoparticle experiment (60 min at 37 °C). Co-cultures incubated in HBSS were used as control. Potassium depletion: nanoparticles suspended in HBSS devoid of potassium were incubated with cell monolayers for 1 h at 37 °C ($n = 4$). Co-cultures incubated in HBSS were used as control. The number of transported nanoparticles was evaluated by flow cytometry. Values are expressed as a percentage of transported nanoparticles by co-cultures in the presence of inhibitor compared with the number of transported nanoparticles by co-cultures in HBSS. (a) $P < 0.05$ vs. the control.

The results of these experiments are summarized in Fig. 8. EIPA reduced nanoparticle transport by 99% and nystatin by 78%, compared to the control ($P < 0.05$). This conclusion is consistent with results previously obtained by Ragnarsson (2006) working with a FAE model obtained by Caco-2 cell incubation with *Yersinia pseudotuberculosis*. However, the potassium depletion conditions used for this experiment did not modify the nanoparticle transport rate, suggesting that nanoparticle endocytosis by M cells is not a clathrin-dependent process. The possible cytotoxicity during incubation with endocytosis inhibitors, evaluated by measuring the LDH activity released from the cytosol of damaged cells into the apical medium after the transport experiments, remained below 5% of the total activity. These results suggest that uptake of 200 nm model carboxylated polystyrene nanoparticles by M cells occurs by non-specific absorptive endocytosis, through a non-clathrin dependent route, most likely macropinocytosis.

4. Conclusion

Since *in vitro* models are currently almost the only tools for studying human M cells, it seems extremely important that they should be characterized as much as possible. Characterization of the inverted *in vitro* model of human FAE revealed the presence of Raji cells in co-culture cell monolayers and allowed the identification of cells morphologically similar to M cells. Morphologic analysis also permitted, for the first time, estimation of the percentage of M cells in the co-cultures (between 15 and 30%). This information is crucial to interpret results and to compare them with *in vivo* data as well as to better characterize the model. Indeed, expressed as a percentage of M cells in the total FAE, rabbits and pigs are well-endowed at 30–50% (Jepson et al., 1993; Gebert et al., 1994). By contrast, there are proportionally fewer M cells in the Peyer's patches of rodents: 10% (Clark et al., 1993, 1994) and humans: <10% (Owen and Ermak, 1990). Hence, the nanoparticle transport results obtained with this model may overestimate the situation in humans, but, nevertheless, the inverted model is a useful tool to study the influence of M cells on nanoparticle transport.

The characterization and comparison of the inverted *in vitro* model of human FAE with the normally oriented model demonstrates the importance of B lymphocytes (Raji cells) on Caco-2 cell conversion. Close contact is not mandatory to obtain a functional model but direct contact of Caco-2 and Raji cells, as well as the concentration of Raji cells at the basolateral pole of Caco-2 cells, seemed to induce a more functional and more reproducible *in vitro* model. In addition, close contact between Caco-2 and Raji cells reproduces *in vivo* FAE organization more faithfully.

With regard the transport of carboxylated nanoparticles, mechanistic studies showed that their transport by M cells occurs by the transcellular route and is energy-dependent. Transport inhibition by EIPA or nystatin, but not by potassium depletion, suggested that M cells take up 200 nm carboxylated polystyrene nanoparticles by non-specific absorption endocytosis, requiring an intact microtubule network, most likely macropinocytosis. However, these data were obtained with model nanoparticles. For future drug delivery applica-

tions, it would be worth checking whether different carriers are transported by M cells by the same pathway, since the properties of nanoparticles influence their uptake by M cells. Indeed, previous work studying the influence of nanoparticle surface properties on their transport by M cells showed the impact of nanoparticle surface hydrophobicity (des Rieux et al., 2005). In addition, Alonso-Sande et al. (2006) have demonstrated that the transport of chitosan and chitosan-glucomannan nanoparticles by M cells occurs via a different mechanism compared to polystyrene model nanoparticles. It is also probable that grafting an M cell targeting molecule to the nanoparticle surface could improve M cell oral delivery strategies by influencing the endocytic mechanisms involved in their uptake by M cells (des Rieux et al., 2006).

Acknowledgements

The authors thank Dr. D. Perez-Morga from the Department of Molecular Biology, Université Libre de Bruxelles for its scientific and technical support in the realization of confocal analysis, as well as Dr. D. Tyteca from the Department of Biochemistry and Cell Biology, Université Catholique de Louvain, and Dr. E.G.E. Ragnarsson, from Department of Pharmacy, Uppsala University, for their precious help and knowledge sharing. The authors wish to thank A. Tonon from the Ludwig Institute Cancer Research for his support in the realization of FACScan analysis as well as Dr. E. Ferain from the Laboratory of Chemistry and Physics of Polymers, Université Catholique de Louvain for his realization of the SEM pictures. P. Camby and M. Stevens from the Department of Pathology, Cliniques Universitaires Saint-Luc, Université Catholique de Louvain are thanked for their help in the realization of the immunohistochemistry analysis. We thank Dr. G. Krack, as well as and C. Hind, from Baxter R&D Europe for the processing of samples for SEM analysis. B. Ucakar is acknowledged for his technical support as well as J.-P. Vandiest for his help with the figures. The authors will at last thank Drs. J. Van Gelder and M. Oth from Lilly® for interest and support of the project. This work was supported by the Region Wallonne (DGTRE), First Europe (nos. 215099 and 415847) and VACCINOR project (WINOMAT), by the Fond Scientifique de Recherche of the Université Catholique de Louvain and by Fonds de la recherche scientifique médicale.

REFERENCES

- Alonso-Sande, M., des Rieux, A., Schneider, Y.J., Remunan-Lopez, C., Alonso, M.J., Preat, V., 2006. Uptake studies of chitosan and chitosan-glucomannan nanoparticles in human intestinal FAE Model. In: Proceedings of the 33rd Annual Meeting of the Controlled Release Society, Vienna.
- Artursson, P., Lindmark, T., Davis, S.S., Illum, L., 1994. Effect of chitosan on the permeability of monolayers of intestinal epithelial cells (Caco-2). *Pharm. Res.* 11, 1358–1361.
- Artursson, P., Palm, K., Luthman, K., 2001. Caco-2 monolayers in experimental and theoretical predictions of drug transport. *Adv. Drug Del. Rev.* 46, 27–43.
- Beaumelle, B.D., Gibson, A., Hopkins, C.R., 1990. Isolation and preliminary characterization of the major membrane boundaries of the endocytic pathway in lymphocytes. *J. Cell Biol.* 111, 1811–1823.
- Beier, R., Gebert, A., 1998. Kinetics of particle uptake in the domes of Peyer's patches. *Am. J. Physiol. Gastrointest. Liver Physiol.* 275, G130.
- Brayden, D.J., 2001. Oral vaccination in man using antigens in particles: current status. *Eur. J. Pharm. Sci.* 14, 183–189.
- Brayden, D.J., Baird, A.W., 2001. Microparticle vaccine approaches to stimulate mucosal immunisation. *Microbes Infect.* 3, 867–876.
- Clark, M.A., Jepson, M.A., Simmons, N.L., Booth, T.A., Hirst, B.H., 1993. Differential expression of lectin-binding sites defines mouse intestinal M-cells. *J. Histochem. Cytochem.* 41, 1679–1687.
- Clark, M.A., Jepson, M.A., Simmons, N.L., Hirst, B.H., 1994. Differential surface characteristics of M cells from mouse intestinal Peyer's and caecal patches. *Histochem. J.* 26, 271–280.
- Clark, M.A., Hirst, B.H., Jepson, M.A., 2000. Lectin-mediated mucosal delivery of drugs and microparticles. *Adv. Drug Del. Rev.* 43, 207–223.
- des Rieux, A., Ragnarsson, E.G.E., Gullberg, E., Pr at, V., Schneider, Y.J., Artursson, P., 2005. Transport of nanoparticles across an in vitro model of the human intestinal follicle associated epithelium. *Eur. J. Pharm. Sci.* 25, 455–465.
- des Rieux, A., Fievez, V., Garinot, M., Schneider, Y.-J., Pr at, V., 2006. Nanoparticles as potential oral delivery systems of proteins and vaccines: a mechanistic approach. *J. Contr. Rel.*, Available online 23 August.
- Ellinger, I., Klapper, H., Courtoy, P.J., Vaerman, J.P., Fuchs, R., 2002. Different temperature sensitivity of endosomes involved in transport to lysosomes and transcytosis in rat hepatocytes: analysis by free-flow electrophoresis. *Electrophoresis* 23, 2117–2129.
- Fallman, M., Gustavsson, A., 2005. Cellular mechanisms of bacterial internalization counteracted by Yersinia. *Int. Rev. Cytol.* 246, 135–188.
- Frey, A., Giannasca, K.T., Weltzin, R., Giannasca, P.J., Reggio, H., Lencer, W.I., Neutra, M.R., 1996. Role of the glycocalyx in regulating access of microparticles to apical plasma membranes of intestinal epithelial cells: implications for microbial attachment and oral vaccine targeting. *J. Exp. Med.* 184, 1045–1059.
- Frey, A., Neutra, M.R., 1997. Targeting of Mucosal Vaccines to Peyer's Patch M Cells. *Behring Institute Mitteilungen*, pp. 376–389.
- Gebert, A., 1997. The role of M cells in the protection of mucosal membranes. *Histochem. Cell Biol.* 108, 455–470.
- Gebert, A., Bartels, H., 1995. Ultrastructure and protein transport of M cells in the rabbit cecal patch. *Anat. Rec.* 241, 487–495.
- Gebert, A., Rothkotter, H.J., Pabst, R., 1994. Cytokeratin 18 is an M-cell marker in porcine Peyer's patches. *Cell Tissue Res.* 276, 213–221.
- Gebert, A., Rothkotter, H.J., Pabst, R., 1996. M cells in Peyer's patches of the intestine. *Int. Rev. Cytol.* 167, 91–159.
- Giannasca, P.J., Giannasca, K.T., Leichtner, A.M., Neutra, M.R., 1999. Human intestinal M cells display the sialyl Lewis A antigen. *Infect. Immun.* 67, 946–953.
- Gullberg, E., 2005. Particle transcytosis across the human intestinal epithelium. Thesis. <http://publications.uu.se/theses/spikblad.xsql?dbid=4780>.
- Gullberg, E., Leonard, M., Karlsson, J., Hopkins, A.M., Brayden, D., Baird, A.W., Artursson, P., 2000. Expression of specific markers and particle transport in a new human intestinal M-cell model. *Biochem. Biophys. Res. Commun.* 279, 808–813.
- Honbo, A., Masaoka, Y., Kataoka, M., Sakuma, S.T., Ragnarsson, E.G.E., Artursson, P., Yamashita, S., 2004. Development of an in vitro M-cell model for macromolecule transport. In: Proceedings of the 19th Annual Meeting of JSSX.

- Jepson, M.A., Clark, M.A., Foster, N., Mason, C.M., Bennett, M.K., Simmons, N.L., Hirst, B.H., 1996. Targeting to intestinal M cells. *J. Anat.* 189 (Pt 3), 507–516.
- Jepson, M.A., Simmons, N.L., Savidge, T.C., James, P.S., Hirst, B.H., 1993. Selective binding and transcytosis of latex microspheres by rabbit intestinal M cells. *Cell Tissue Res.* 271, 399–405.
- Jones, B.D., Ghori, N., Falkow, S., 1994. Salmonella typhimurium initiates murine infection by penetrating and destroying the specialized epithelial M cells of the Peyer's patches. *J. Exp. Med.* 180, 15–23.
- Kerneis, S., Bogdanova, A., Kraehenbuhl, J.P., Pringault, E., 1997. Conversion by Peyer's patch lymphocytes of human enterocytes into M cells that transport bacteria. *Science* 277, 949–952.
- Knipp, G.T., Ho, N.F., Barsuhn, C.L., Borchardt, R.T., 1997. Paracellular diffusion in Caco-2 cell monolayers: effect of perturbation on the transport of hydrophilic compounds that vary in charge and size. *J. Pharm. Sci.* 86, 1105–1110.
- Larkin, J.M., Brown, M.S., Goldstein, J.L., Anderson, R.G., 1983. Depletion of intracellular potassium arrests coated pit formation and receptor-mediated endocytosis in fibroblasts. *Cell* 33, 273–285.
- Liu, N.Q., Lossinsky, A.S., Popik, W., Li, X., Gujuluva, C., Kriederman, B., Roberts, J., Pushkarsky, T., Bukrinsky, M., Witte, M., Weinand, M., Fiala, M., 2002. Human immunodeficiency virus type 1 enters brain microvascular endothelia by macropinocytosis dependent on lipid rafts and the mitogen-activated protein kinase signaling pathway. *J. Virol.* 76, 6689–6700.
- Liu, S.M., Magnusson, K.E., Sundqvist, T., 1993. Microtubules are involved in transport of macromolecules by vesicles in cultured bovine aortic endothelial cells. *J. Cell Physiol.* 156, 311–316.
- Madshus, I.H., Sandvig, K., Olsnes, S., van, D.B., 1987a. Effect of reduced endocytosis induced by hypotonic shock and potassium depletion on the infection of Hep 2 cells by picornaviruses. *J. Cell Physiol.* 131, 14–22.
- Madshus, I.H., Tonnessen, T.I., Olsnes, S., Sandvig, K., 1987b. Effect of potassium depletion of Hep 2 cells on intracellular pH and on chloride uptake by anion antiport. *J. Cell Physiol.* 131, 6–13.
- Mast, J., Nanbru, C., van den, B.T., Meulemans, G., 2005. Ultrastructural changes of the tracheal epithelium after vaccination of day-old chickens with the La Sota strain of Newcastle disease virus. *Vet. Pathol.* 42, 559–565.
- Mounier, J., Vasselon, T., Hellio, R., Lesourd, M., Sansonetti, P.J., 1992. Shigella flexneri enters human colonic Caco-2 epithelial cells through the basolateral pole. *Infect. Immun.* 60, 237–248.
- Neutra, M.R., Sansonetti, P.J., Kraehenbuhl, J., 2003. M Cells and Microbial Pathogens. Raven Press, pp. 163–178.
- Niedergang, F., Kraehenbuhl, J., 2000. Much ado about M cells. *Trends Cell Biol.* 10, 137–141.
- Owen, R.L., 1977. Sequential uptake of horseradish peroxidase by lymphoid follicle epithelium of Peyer's patches in the normal unobstructed mouse intestine: an ultrastructural study. *Gastroenterology* 72, 440–451.
- Owen, R.L., Ermak, T.H., 1990. Structural specializations for antigen uptake and processing in the digestive tract. *Springer Semin. Immunopathol.* 12, 139–152.
- Peachman, K.K., Rao, M., Palmer, D.R., Zidanic, M., Sun, W., Alving, C.R., Rothwell, S.W., 2004. Functional microtubules are required for antigen processing by macrophages and dendritic cells. *Immunol. Lett.* 95, 13–24.
- Pizarro-Cerda, J., Cossart, P., 2004. Subversion of phosphoinositide metabolism by intracellular bacterial pathogens. *Nat. Cell Biol.* 6, 1026–1033.
- Ragnarsson, E.G.E., 2006. Effects of microparticles drug delivery systems: tissue responses and transcellular transport. Thesis. <http://publications.uu.se/theses/spikblad.xsql?dbid=6260>.
- Rescigno, M., Urbano, M., Valzasina, B., Francolini, M., Rotta, G., Bonasio, R., Granucci, F., Kraehenbuhl, J.P., Ricciardi-Castagnoli, P., 2001. Dendritic cells express tight junction proteins and penetrate gut epithelial monolayers to sample bacteria. *Nat. Immunol.* 2, 361–367.
- Riley, S.A., Warhurst, G., Crowe, P.T., Turnberg, L.A., 1991. Active hexose transport across cultured human Caco-2 cells: characterisation and influence of culture conditions. *Biochim. Biophys. Acta* 1066, 175–182.
- Sakai, M., Imai, T., Ohtake, H., Azuma, H., Otagiri, M., 1997. Effects of absorption enhancers on the transport of model compounds in Caco-2 cell monolayers: assessment by confocal laser scanning microscopy. *J. Pharm. Sci.* 86, 779–785.
- Schulte, R., Kerneis, S., Klinke, S., Bartels, H., Preger, S., Kraehenbuhl, J.P., Pringault, E., Autenrieth, I.B., 2000. Translocation of Yersinia enterocolitica across reconstituted intestinal epithelial monolayers is triggered by Yersinia invasin binding to beta1 integrins apically expressed on M-like cells. *Cell Microbiol.* 2, 173–185.
- Sergent, T., Parys, M., Garsou, S., Pussemier, L., Schneider, Y.J., Larondelle, Y., 2006. Deoxynivalenol transport across human intestinal Caco-2 cells and its effects on cellular metabolism at realistic intestinal concentrations. *Toxicol. Lett.* 164, 167–176.
- Wadia, J.S., Stan, R.V., Dowdy, S.F., 2004. Transducible TAT-HA fusogenic peptide enhances escape of TAT-fusion proteins after lipid raft macropinocytosis. *Nat. Med.* 10, 310–315.
- Zaro, J.L., Shen, W.C., 2005. Evidence that membrane transduction of oligoarginine does not require vesicle formation. *Exp. Cell Res.* 307, 164–173.